Astronomy & Astrophysics manuscript no. eb
June 19, 2014
©ESO 2014

arXiv:1406.0645v2 [astro-ph.HE] 18 Jun 2014

Letter to the Editor

TANAMI blazars in the IceCube PeV neutrino fields

F. Krauß[1,2], M. Kadler[2], K. Mannheim[2], R. Schulz[1,2], J. Trüstedt[1,2], J. Wilms[1], R. Ojha[3,4,5], E. Ros[6,7,8], G. Anton[9], W. Baumgartner[3], T. Beuchert[1,2], J. Blanchard[10], C. Bürkel[1,2], B. Carpenter[5], T. Eberl[9], P.G. Edwards[11], D. Eisenacher[2], D. Elsässer[2], K. Fehn[9], U. Fritsch[9], N. Gehrels[3], C. Gräfe[1,2], C. Großberger[12], H. Hase[13], S. Horiuchi[14], C. James[9], A. Kappes[2], U. Katz[9], A. Kreikenbohm[1,2], I. Kreykenbohm[1], M. Langejahn[1,2], K. Leiter[1,2], E. Litzinger[1,2], J.E.J. Lovell[15], C. Müller[1,2], C. Phillips[11], C. Plötz[13], J. Quick[16], T. Steinbring[1,2], J. Stevens[11], D. J. Thompson[3], and A.K. Tzioumis[11]

(Affiliations can be found after the references)

Received 15 May 2014 / Accepted 2 June 2014

ABSTRACT

The IceCube Collaboration has announced the discovery of a neutrino flux in excess of the atmospheric background. Owing to the steeply falling atmospheric background spectrum, events at PeV energies most likely have an extraterrestrial origin. We present the multiwavelength properties of the six radio-brightest blazars that are positionally coincident with these events using contemporaneous data of the TANAMI blazar sample, including high-resolution images and spectral energy distributions. Assuming the X-ray to γ-ray emission originates in the photoproduction of pions by accelerated protons, the integrated predicted neutrino luminosity of these sources is high enough to explain the two detected PeV events.

Key words. neutrinos – galaxies: active – quasars: general

1. Introduction

The detection of neutrinos at PeV energies in excess of the atmospheric background reported by the IceCube Collaboration (Aartsen et al. 2013; IceCube Collaboration 2013) has prompted a quest to identify their extraterrestrial sources. The two events with PeV energies (event 20, dubbed 'Ernie' and event 14, 'Bert', hereafter E20 and E14), detected between May 2010 and May 2012[1], have angular uncertainties of 10.°7 and 13.°2, respectively.

A Galactic center origin has been considered (Razzaque 2013), but a single source has been excluded by Adrián-Martínez et al. (2014). Pevatrons in the Galactic center region, such as young supernova remnants, produce neutrinos at well below 1 PeV (Aharonian & Atoyan 1996). The overall distribution of all 28 IceCube events is consistent with an isotropic source population, and therefore extragalactic sources are the prime suspects. Neutrino emission has been theoretically predicted from the cores of active galactic nuclei (AGN) (Stecker 2013), AGN jets (Mannheim 1995), or gamma-ray bursts (Waxman & Bahcall 1997). Prevailing models for gamma-ray bursts have recently been excluded as neutrino sources (Abbasi et al. 2012), and revised models predict much lower neutrino fluxes than the observed excess (Winter 2013). Among the models for a diffuse, isotropic neutrino flux at PeV energies, only the predicted flux of $\sim 10^{-8}$ GeV cm^{-2} s^{-1} sr^{-1} from AGN jets matches the observed excess flux well (Learned & Mannheim 2000), although it does not explain the absence of Glashow-resonance events and the possible gap between 400 GeV and 1 PeV. AGN jets carry a fraction of the total gravitational energy released during the accretion of matter onto supermassive black holes. If observed at a small angle to the line of sight, the emission becomes relativistically boosted, so the source is classified as a blazar. Their low-energy, non-thermal radiation stems from synchrotron emission. The emission at high energies is explained by hadronic or leptonic models. In hadronic models protons are accelerated and interact with low-energy photons (e.g., accretion disk) to produce pions (pion photoproduction, Mannheim & Biermann 1989). The pion decays and ensuing cascades generate neutrinos and γ rays. Since the observed spectral energy distributions (SEDs) of AGN result from the superposition of many emission zones within the jets, the distinction between hadronic and leptonic emission processes is obscured by the large number of adjustable parameters. Unambiguous evidence of hadronic processes could be provided by neutrino observations.

In this Letter we address the question of whether the PeV neutrinos detected by IceCube could originate in blazars by calculating the expected neutrino fluence. In Sect. 2, we describe multiwavelength data on the six candidate sources. In Sect. 3 we present Very Long Baseline Interferometry (VLBI) images and SEDs and discuss their expected neutrino emission.

2. Observational data

Tracking Active Galactic Nuclei with Austral Milliarcsecond Interferometry (TANAMI)[2] (Ojha et al. 2010) is a multiwavelength program that monitors extragalactic jets of the Southern Sky ($\delta < -30°$). The sample includes the brightest radio- and γ-ray (GeV) blazars. VLBI observations were conducted with the Australian Long Baseline Array (LBA) in combination with telescopes in South Africa, Chile, Antarctica, and New Zealand at

[1] A third neutrino at 2 PeV (event 35, dubbed 'Big Bird') has recently been reported for the third year of data (Aartsen et al. 2014).

[2] `http://pulsar.sternwarte.uni-erlangen.de/tanami/`

8.4 GHz and 22.3 GHz. The DiFX correlator at Curtin University in Perth, Western Australia (Deller et al. 2007, 2011) was used to correlate the data. Subsequent calibration, hybrid imaging, and image analysis were performed following Ojha et al. (2010). TANAMI radio observations are supported by flux-density measurements with the Australia Telescope Compact Array (ATCA) (Stevens et al. 2012) and the Ceduna 30 m telescope (McCulloch et al. 2005).

X-ray data taken during the IceCube period are from the TANAMI program and the public archives of *Swift* (Gehrels et al. 2004) and *XMM-Newton* (Strüder et al. 2001) and were supplemented with non-simultaneous archival data. *Swift*/XRT and *XMM-Newton*/pn data were reduced with standard methods, using the most recent software packages (HEASOFT 6.15.1[3], SAS 1.2.[4]) and calibration databases. Spectra were grouped to a minimum signal-to-noise ratio of 3 for the *Swift*/XRT data and 5 for the *XMM-Newton*/pn data. Spectral fitting was performed with ISIS 1.6.2 (Houck & Denicola 2000) using Cash statistics (Cash 1979), except for the *XMM-Newton* data, where the higher count rates allow using χ^2-statistics. We fitted the 0.5–10 keV energy band with an absorbed power-law model, which yielded good results in all cases. None of the sources showed evidence of intrinsic X-ray absorption in excess of the Galactic value (Kalberla et al. 2005). X-ray data were deabsorbed using abundances from Wilms et al. (2000) and cross sections from Verner et al. (1996). *Swift*/UVOT and *XMM-Newton*/OM data were extracted following standard methods. Optical, infrared, and ultraviolet data were dereddened using the same absorbing columns (Nowak et al. 2012, and references therein). We included spectral data for these six sources from the *Fermi*/LAT (Atwood et al. 2009) second source catalog (Nolan et al. 2012, 2FGL), which covered the time period 2008 August to 2010 August. We also calculated spectra for the 2010 May to 2012 May IceCube integration period using the reprocessed Pass 7 data (v9r32p5) and the P7REP_SOURCE_V15 instrumental response functions (IRF; Ackermann et al. 2012) and a region of interest (ROI) of 7°. Non-simultaneous data from the *Swift*/BAT 70-month catalog (Baumgartner et al. 2013, hard X-rays), *Planck* (Planck Collaboration, et al. 2011, microwave), Wide-Field Infrared Survey Explorer (*WISE*; Wright et al. 2010), and Two Micron All Sky Survey (2MASS; Skrutskie et al. 2006) (infrared) are also included. An *INTEGRAL* (Winkler et al. 2003) spectrum has been obtained for 1653−329 for all available data since 2003 using the HEAVENS online tool (Walter et al. 2010).

3. Results

3.1. TANAMI sources in the two PeV-neutrino fields

Six TANAMI sources are located in the 1σ positional uncertainty region for the two PeV events (Table 1). The three blazars PKS B0235−618 (in the following referred to as 0235−618), PKS B0302−623 (0302−623), and PKS B0308−611 (0308−611) are located in the E20 field. In the E14 field we find the three blazars Swift J1656.3−3302 (1653−329), PMN J1717−3342 (1714−336) and PMN J1802−3940 (1759−396). Of the twelve brightest γ-ray sources (in the two fields) from the 2FGL catalog, only these six named sources have correlated VLBI flux densities at 8.4 GHz above 400mJy. All other sources are considerably fainter with typically 30 mJy to 160 mJy at 1.4 GHz and on kpc scales (Condon et al. 1998). The source 0235−618 is formally also consistent with IceCube event 7 (34.3 TeV), while 1653−329 and 1714−336 are also within the error circles of events 2 (117 TeV) and 25 (33.5 TeV). The source 1759−396 agrees with the positions of events 2 (117 TeV), 15 (57.5 TeV), and 25 (33.5 TeV).

3.2. VLBI images

The TANAMI VLBI jets of 0235−618, 0308−611, and 1759−396 are one-sided, indicating relativistic boosting at small angles to the line of sight (see Fig. 1). The northwest direction of the 0308−611 jet does not agree with the position angle indicated by the VLBI Space Observatory Program (VSOP) image of Dodson et al. (2008), which might be due to jet curvature or the limited (u, v)-coverage of VSOP. The source 0302−623, which appeared point-like in Ojha et al. (2004), shows a highly peculiar morphology with a compact core and a strong halo-like emission region around the core. The east-west extension agrees with Dodson et al. (2008). We find a high brightness temperature[5] of several times 10^{11} K in four objects, which is typical of γ-ray-emitting blazars (Linford et al. 2012). We find that 1714−336 is substantially scatter broadened. The image of 1653−329 is from one single scan in 2008 February, outside the IceCube integration period and does not have the same quality as other TANAMI images.

3.3. Broadband spectra

For all six sources, we find characteristic double-humped blazar SEDs (Fig. 2). The source 1653−329 has an unusually dominant high-energy hump and is bright at hard X-rays (Masetti et al. 2008; Baumgartner et al. 2013), while only upper limits are placed on the 14–195 keV flux by *Swift*/BAT for the other sources, based on the 3σ level of background variations in the survey maps. The high-energy peak frequencies lie between 10^{20} Hz and 10^{22} Hz. 1653−329 and 1714−336, and possibly 1759−396 show an additional component between 10^{14} Hz and 10^{15} Hz, which could be explained by a thermal accretion disk.

4. Discussion

4.1. Possible other AGN sources of the IceCube events

The six TANAMI blazars are the brightest radio and γ-ray emitting AGN in the two IceCube PeV event fields. The two moderately bright extragalactic radio sources PKS 1657−261 and PKS 1741−312 (270 mJy and 470 mJy compact flux density at 8.4 GHz and 8.6 GHz, respectively) with compact jets (Ojha et al. 2004; Petrov et al. 2005; Condon et al. 1998) have not shown substantial γ-ray emission in the 2FGL period. The same is true of several hard X-ray detected blazars and radio galaxies (Baumgartner et al. 2013). Four blazars are slightly outside the uncertainty region of E14: NRAO 530, PKS 1622−29, PKS 1622−253, and PKS 1830−211 at 15.°0, 16.°8, 17.°3, and 13.°5 distance to the coordinates at 13.°2 error radius.

4.2. Expected neutrino rate from pion photoproduction

Proton acceleration occurs in blazar jets moving with bulk Lorentz factor Γ. In pion photoproduction the neutrino flux is

[3] http://heasarc.nasa.gov/lheasoft/
[4] http://xmm.esac.esa.int/sas/

[5] We derived brightness temperatures following Kovalev et al. (2005) from Gaussian model fits to the visibility data.

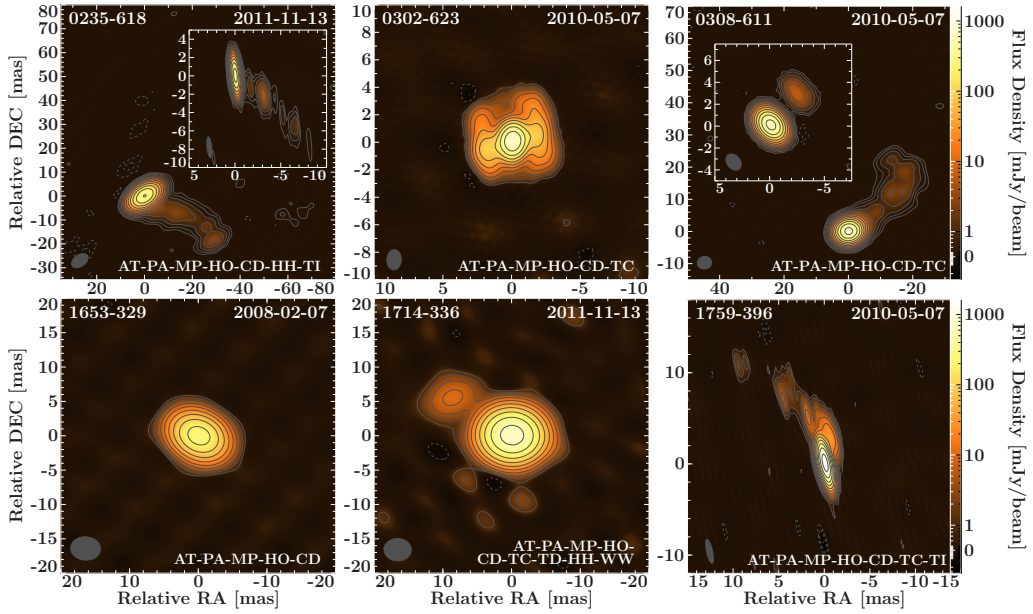

Fig. 1. VLBI images at 8.4 GHz (natural weighting for insets of 0235−618 and 0308−611 and all other images; tapered to 10% at 100 Mλ for main panels of 0235−618 and 0308−611). Restoring beams are shown in the bottom left corners. The color scale covers the range between the mean noise level and the maximum flux density (1759−396, see Table 2 for image parameters). Contour lines start at $3\sigma_{\rm rms}$ and increase logarithmically by factors of 2. The array is given in the bottom right corner: PA: Parkes, AT: ATCA, MP: Mopra, HO: Hobart, CD: Ceduna, HH: Hartebeesthoek, TC: Tigo, TI: Tidbinbilla (70 m), TD: Tidbinbilla (34 m), WW:Warkworth

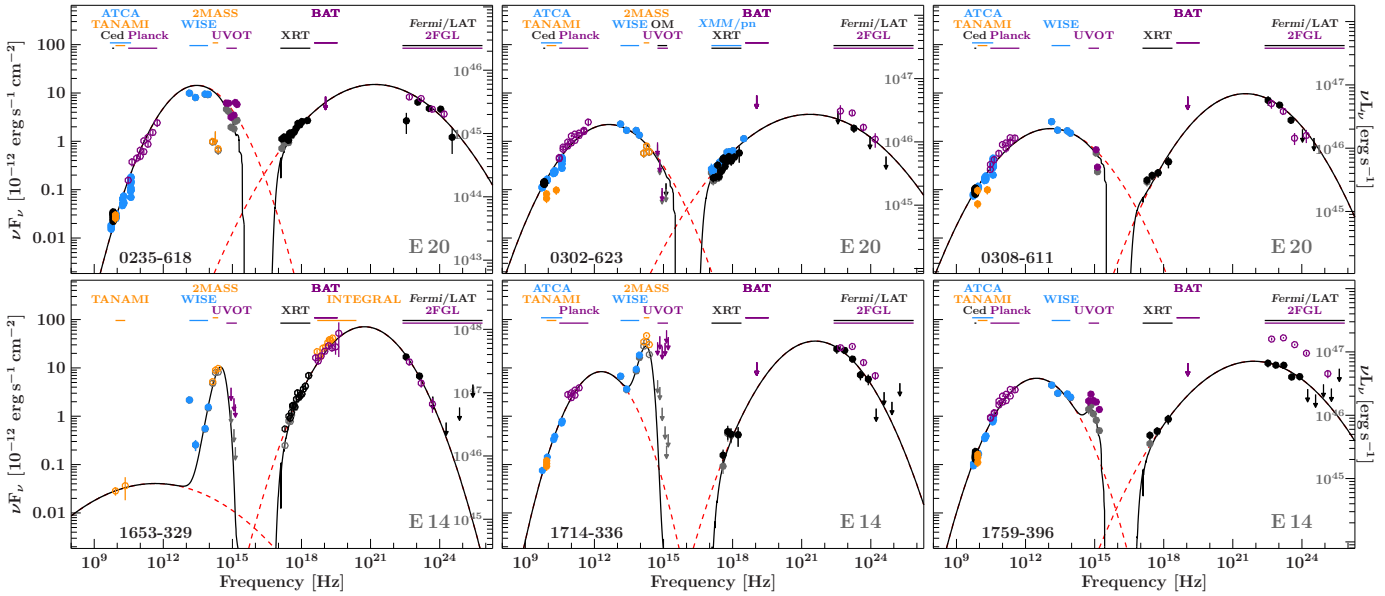

Fig. 2. Broadband SEDs for the six TANAMI blazars. Filled data points are from the IceCube integration period (2010 May–2012 May), open circles are archival data outside the time period. Gray shows the absorbed (X-ray) and reddened (optical/UV) spectra. The data have been parametrized with logarithmic parabolas (red dashed lines) modified by extinction and absorption, as well as by an additional blackbody component where necessary (black solid lines).

related to the bolometric high-energy electromagnetic flux. We consider the illustrative case of isospin symmetry (equal numbers of π^+, π^-, and π°). We obtain the neutrino flux for the three neutrinos among the four light final-state leptons in charged pion decays $F_\nu = 2/3 \cdot 3/4 \cdot F_\pi = 1/2 \cdot F_\pi$, and the γ-ray flux after accounting for the conversion of electrons and positrons into γ rays by cascading, $F_\gamma = 1/3 \cdot F_\pi + 1/4 \cdot 2/3 \cdot F_\pi = 1/2 \cdot F_\pi$ and therefore $F_\nu = F_\gamma$. Monte-Carlo simulations confirm this simple estimate (Mücke et al. 2000). Neutrino oscillations establish full-flavor mixing across extragalactic distance scales, and therefore $F_{\rm b,\nu_e} = F_{\rm b,\nu}/3 = F_{\rm b,\gamma}/3$. Electromagnetic cascades emerge at X-ray and γ-ray energies, and we approximate the non-thermal bolometric photon flux F_γ by the integrated flux between 1 keV and 5 GeV. The broadband spectra were fit with two logarithmic parabolas (Massaro et al. 2004), as well as a blackbody component, X-ray absorption and optical extinction. This fit was then integrated in the given energy range. All but one of the blazars in our sample belong to the FSRQ class, showing strong emission lines due to photo-ionizing UV light from an accretion disk that could provide target photons. The exception is 1714−336, which has been classified as a BL Lac object (Véron-Cetty & Véron 2006) but shows a particularly strong big blue bump in the UV and is possibly a misclassified quasar. In the jet's comoving frame (marked with primed quantities), the UV photons from the disk are redshifted ($\epsilon' = \epsilon/\Gamma$) if they originate at the base of the jet, or blueshifted if they come from the outer parts of the disk or are scattered photons. Photoproduction of pions starts above the threshold energy $E'_{\rm p,th} = 2(\epsilon'/30\,{\rm eV})^{-1}$ PeV. The neutrinos carry away $\sim 5\%$ of the proton energy, implying a neutrino energy of $E_\nu \sim 0.1\Gamma(\epsilon'/30\ {\rm eV})^{-1}$ PeV in the observer's frame. For generic values $\epsilon = 30$ eV and $\Gamma = 10$, the neutrino spectrum covers the energy range from 100 TeV to 10 PeV. Details of the spectrum,

however, are subject to model assumptions and beyond the scope of this paper. IceCube would have measured the following number of electron neutrino events $N_{\nu_e}(E_\nu) \simeq A_{\rm eff}(E_\nu)(F_{\nu_e}/E_\nu)\Delta t$. Adopting $E_\nu = 1\,$PeV as the neutrino-production peak energy, an exposure time of $\Delta t = 662\,$days, and an effective area of $A_{\rm eff} = 10^5\,{\rm cm}^2$ for contained PeV events, we obtain the values listed in Table 3. The numbers would be lower for a realistic spectrum of the emitted neutrinos or if some fraction of the emission were of a leptonic, proton-synchrotron, or Bethe-Heitler origin. The steepness of the blazar γ-ray luminosity function (Singal et al. 2012), implies that in a large field, the neutrino fluence will have significant contributions from the brightest sources in the field, as well as from fainter, unresolved sources.

5. Conclusions

The six candidate sources from the TANAMI sample are the radio-brightest blazars in the neutrino error fields. Assuming that the high-energy emission stems from pion photoproduction due to accelerated protons, the maximum expected number of electron neutrino events from the six blazars in 662 days is 1.9 ± 0.4. This is surprisingly close to the actual number of observed events, given the additional neutrinos expected from a large number of remote, faint blazars not included in the TANAMI sample. The most promising candidate sources are the three TANAMI blazars in the E14 field, with the highest predicted neutrino rates and the prevalence of blue bumps. The detection statistics of neutrinos at these low fluxes is expected to be Poisson-distributed. For N=1, the 1σ single-sided lower and upper limits are 0.173 and 3.300, respectively. With a predicted neutrino fluence of 0.39/1.55 events for the E20/E14 field, we are well inside the Poisson uncertainty ranges. The six TANAMI sources alone are already capable of producing the observed PeV neutrino flux.

Acknowledgements. We thank the referee for the helpful comments. We acknowledge support and partial funding by the Deutsche Forschungsgemeinschaft grant WI 1860-10/1 (TANAMI) and GRK 1147, Deutsches Zentrum für Luft- und Raumfahrt grant 50 OR 1311/50 OR 1103, and the Helmholtz Alliance for Astroparticle Physics (HAP). E. R. was partially supported by the Spanish MINECO projects AYA2009-13036-C02-02, and AYA2012-38491-C02-01 and by the Generalitat Valenciana project PROMETEO/2009/104, as well as by the COST MP0905 action "Black Holes in a Violent Universe". We thank J.E. Davis and T. Johnson for the development of the `slxfig` module and the SED scripts that have been used to prepare the figures in this work. This research has made use of a collection of ISIS scripts provided by the Dr. Karl Remeis-Observatory, Bamberg, Germany at `http://www.sternwarte.uni-erlangen.de/isis/`. The Long Baseline Array and Australia Telescope Compact Array are part of the Australia Telescope National Facility, which is funded by the Commonwealth of Australia for operation as a National Facility managed by CSIRO. The *Fermi*-LAT Collaboration acknowledges support for LAT development, operation and data analysis from NASA and DOE (United States), CEA/Irfu and IN2P3/CNRS (France), ASI and INFN (Italy), MEXT, KEK, and JAXA (Japan), and the K.A. Wallenberg Foundation, the Swedish Research Council, and the National Space Board (Sweden). Science analysis support in the operations phase from INAF (Italy) and CNES (France) is also gratefully acknowledged.

References

Aartsen M.G., Abbasi R., Abdou Y., et al., 2013, Phys. Rev. Lett. 111, 021103
Abbasi R., Abdou Y., Abu-Zayyad T., et al., 2012, Nat 484, 351
Ackermann M., Ajello M., Albert A., et al., 2012, ApJS 203, 4
Adrián-Martínez S., Albert A., André M., et al., 2014, ApJL 786, L5
Aharonian F.A., Atoyan A.M., 1996, A&A 309, 917
Atwood W.B., Abdo A.A., Ackermann M., et al., 2009, ApJ 697, 1071
Baumgartner W.H., Tueller J., Markwardt C.B., et al., 2013, ApJS 207, 19
Cash W., 1979, ApJ 228, 939
Condon J.J., Cotton W.D., Greisen E.W., et al., 1998, AJ 115, 1693
Cutri R.M., Skrutskie M.F., van Dyk S., et al., 2003, VizieR Online Data Catalog 2246
Deller A.T., Brisken W.F., Phillips C.J., et al., 2011, PASP 123, 275
Deller A.T., Tingay S.J., Bailes M., West C., 2007, PASP 119, 318
Dodson R., Fomalont E.B., Wiik K., et al., 2008, ApJS 175, 314
Fomalont E.B., Petrov L., MacMillan D.S., et al., 2003, AJ 126, 2562
Gehrels N., Chincarini G., Giommi P., et al., 2004, ApJ 611, 1005
Healey S.E., Romani R.W., Cotter G., et al., 2008, ApJS 175, 97
Houck J.C., Denicola L.A., 2000, In: Manset N., Veillet C., Crabtree D. (eds.) Astronomical Data Analysis Software and Systems IX, 216. Astronomical Society of the Pacific Conference Series, p. 591
IceCube Collaboration 2013, Science 342, 6161, 1242856
Immer K., Brunthaler A., Reid M.J., et al., 2011, ApJS 194, 25
Kalberla P.M.W., Burton W.B., Hartmann D., et al., 2005, A&A 440, 775
Kovalev Y.Y., Kellermann K.I., Lister M.L., et al., 2005, AJ 130, 2473
Lambert S.B., Gontier A.M., 2009, A&A 493, 317
Learned J.G., Mannheim K., 2000, Annual Review of Nuclear and Particle Science 50, 679
Linford J.D., Taylor G.B., Schinzel F.K., 2012, ApJ 757, 25
Mannheim K., 1995, Astroparticle Physics 3, 295
Mannheim K., Biermann P.L., 1989, A&A 221, 211
Masetti N., Mason E., Landi R., et al., 2008, A&A 480, 715
Massaro E., Giommi P., Leto C., et al., 2009, A&A 495, 691
Massaro E., Perri M., Giommi P., Nesci R., 2004, A&A 413, 489
McCulloch P.M., Ellingsen S.P., Jauncey D.L., et al., 2005, AJ 129, 2034
Mücke A., Rachen J.P., Engel R., et al., 2000, Nuclear Physics B Proceedings Supplements 80, C810
Nolan P.L., Abdo A.A., Ackermann M., et al., 2012, ApJS 199, 31
Nowak M.A., Neilsen J., Markoff S.B., et al., 2012, ApJ 759, 95
Ojha R., Fey A.L., Johnston K.J., et al., 2004, AJ 127, 3609
Ojha R., Kadler M., Böck M., et al., 2010, A&A 519, A45
Petrov L., Kovalev Y.Y., Fomalont E., Gordon D., 2005, AJ 129, 1163
Planck Collaboration, Ade P.A.R., Aghanim N., et al., 2011, A&A 536, A7
Razzaque S., 2013, Phys. Rev. D 88, 081302
Singal J., Petrosian V., Ajello M., 2012, ApJ 753, 45
Skrutskie M.F., Cutri R.M., Stiening R., et al., 2006, AJ 131, 1163
Stecker F.W., 2013, Phys. Rev. D 88, 047301
Stevens J., Edwards P.G., Ojha R., et al., 2012, In: Fermi & Jansky Proceedings: Our Evolving Understanding of AGN., arXiv:1205.2403
Strüder L., Briel U., Dennerl K., et al., 2001, A&A 365, L18
Verner D.A., Ferland G.J., Korista K.T., Yakovlev D.G., 1996, ApJ 465, 487
Véron-Cetty M.P., Véron P., 2006, A&A 455, 773
Walter R., Rohlfs R., Meharga M.T., et al., 2010, In: Eighth Integral Workshop. The Restless Gamma-ray Universe (INTEGRAL 2010).
Waxman E., Bahcall J., 1997, Physical Review Letters 78, 2292
Wilms J., Allen A., McCray R., 2000, ApJ 542, 914
Winkler C., Courvoisier T.J.L., Di Cocco G., et al., 2003, A&A 411, L1
Winter W., 2013, Phys. Rev. D 88, 083007
Wright E.L., Eisenhardt P.R.M., Mainzer A.K., et al., 2010, AJ 140, 1868

[1] Dr. Remeis Sternwarte & ECAP, Universität Erlangen-Nürnberg, Sternwartstrasse 7, 96049 Bamberg, Germany
[2] Institut für Theoretische Physik und Astrophysik, Universität Würzburg, Emil-Fischer-Str. 31, 97074 Würzburg, Germany
[3] NASA, Goddard Space Flight Center, Greenbelt, MD 20771, USA
[4] University of Maryland, Baltimore County, Baltimore, MD 21250, USA
[5] Catholic University of America, Washington, DC 20064, USA
[6] Max-Planck-Institut für Radioastronomie, Auf dem Hügel 69, 53121 Bonn, Germany
[7] Departament d'Astronomia i Astrofísica, Universitat de València, C/ Dr. Moliner 50, 46100 Burjassot, València, Spain
[8] Observatori Astronòmic, C/ Catedrático José Beltrán no. 2, 46980 Paterna, València, Spain
[9] ECAP, Universität Erlangen-Nürnberg, Erwin-Rommel-Str. 1, 91058 Erlangen, Germany
[10] Departamento de Astronomía, Universidad de Concepción, Casilla 160, Chile
[11] CSIRO Astronomy and Space Science, ATNF, PO Box 76 Epping, NSW 1710, Australia
[12] Max-Planck-Institut für extraterrestrische Physik, Giessenbachstraße 1, 85741 Garching, Germany Bonn, Germany
[13] Bundesamt für Kartographie und Geodäsie, 93444 Bad Kötzting, Germany
[14] CSIRO Astronomy and Space Science, Canberra Deep Space Communications Complex, P.O. Box 1035, Tuggeranong, ACT 2901, Australia
[15] School of Mathematics & Physics, University of Tasmania, Private Bag 37, Hobart, Tasmania 7001, Australia
[16] Hartebeesthoek Radio Astronomy Observatory, Krugersdorp, South Africa

Table 1. TANAMI sources compatible with the two IceCube PeV events.

Source	R.A.[°]	De.c[°]	z	Class.	Θ [°]
0235−618	39.2218$^{\triangle}$	−61.6043$^{\triangle}$	0.47$^{\blacklozenge}$	FSRQ$^{\blacklozenge}$	5.61
0302−623	45.9610†	−62.1904†	1.35$^{\blacklozenge}$	FSRQ$^{\blacklozenge}$	5.98
0308−611	47.4838†	−60.9775†	1.48$^{\blacklozenge}$	FSRQ$^{\blacklozenge}$	7.39
1653−329	254.0699$^{\triangle}$	−33.0369$^{\triangle}$	2.40$^{\diamond}$	FSRQ$^{\diamond}$	11.18
1714−336	259.4001*	−33.7024*	?	BL Lac$^{\blacktriangle}$	7.87
1759−396	270.6778$^{\bullet}$	−39.6689$^{\bullet}$	1.32$^{\blacksquare}$	FSRQ$^{\blacksquare}$	12.50

Notes. Columns: (1) IAU B1950 name, (2) right ascension, (3) declination, (4) redshift, (5) optical classification, (6) angular distance to IceCube event coordinates
$^{\blacklozenge}$ Healey et al. (2008), $^{\triangle}$ Cutri et al. (2003), † Lambert & Gontier (2009), * Immer et al. (2011), $^{\bullet}$ Fomalont et al. (2003), $^{\blacktriangle}$ Véron-Cetty & Véron (2006), $^{\blacksquare}$ Massaro et al. (2009), $^{\diamond}$ Masetti et al. (2008)

Table 2. Details of interferometric observations and image parameters

Source	ν	$S_{\rm peak}{}^{a}$	$\sigma_{\rm rms}{}^{a}$	$S_{\rm total}{}^{a}$	T_B	Beam^{a}
0235−618	8.4	0.32	0.08	0.38	1.6	0.51×2.28, 5.8
		(0.35)	(0.06)	(0.37)		$(4.85 \times 7.70, -54.9)$
0302−623	8.4	0.83	0.29	1.38	1.9	1.05×1.47, −2.8
	22.3	0.45	0.12	0.69	1.2	1.59×2.28, 87.6
0308−611	8.4	0.68	0.09	0.77	2.0	1.20×1.64, 38.8
		(0.73)	(0.05)	(0.77)		$(3.89 \times 4.49, -80.9)$
	22.3	0.50	0.13	0.54	0.3	1.53×1.82, −75.9
1653−329	8.4	0.28	0.26	0.34	0.1	3.38×4.33, 86.8
	22.3	–^{b}	–^{b}	0.17^{b}		–^{b}
1714−336	8.4	0.74	0.36	1.27	0.02^{c}	3.26×3.98, 87.8
1759−396	8.4	1.63	0.18	2.01	3.1	0.64×2.70, 12.2
	22.3	1.12	0.18	1.19	0.2	1.47×4.32, 78.4

Notes. Columns: (1) IAU B1950 source name, (2) observing frequency in GHz, (3) peak flux density in Jy/beam, (4) image noise level in mJy/beam, (5) total flux density in Jy (uncertainties are $\lesssim$ 10 % and $\lesssim$ 20 % at 8.4 GHz and 22.3 GHz), (6) minimum core brightness temperature in 10^{11} K and (7) restoring beam (size, position angle) in mas^2 and degree. $^{(a)}$ Values in brackets denote the application of a Gaussian taper to the visibility data of 10 % at a baseline length of 100 Mλ. $^{(b)}$ One baseline experiment, flux density only accurate to ∼50%.^{c} $z = 0$ assumed, affected by interstellar scattering broadening.

Table 3. Integrated electromagnetic energy flux from 1 keV to 5 GeV and expected electron neutrino events at 1 PeV in 662 days of IceCube data for the six candidate blazars. Errors are statistical only.

Source	F_γ(erg cm^{-2} s^{-1})	events
0235−618	$\left(1.0^{+0.5}_{-0.5}\right) \times 10^{-10}$	$0.19^{+0.04}_{-0.04}$
0302−623	$\left(3.4^{+0.7}_{-0.7}\right) \times 10^{-11}$	$0.06^{+0.01}_{-0.01}$
0308−611	$\left(7.5^{+2.9}_{-2.9}\right) \times 10^{-11}$	$0.14^{+0.05}_{-0.05}$
1653−329	$\left(4.5^{+0.5}_{-0.5}\right) \times 10^{-10}$	$0.86^{+0.10}_{-0.10}$
1714−336	$\left(2.4^{+0.5}_{-0.6}\right) \times 10^{-10}$	$0.46^{+0.10}_{-0.12}$
1759−396	$\left(1.2^{+0.3}_{-0.2}\right) \times 10^{-10}$	$0.23^{+0.50}_{-0.40}$
Total		1.9 ± 0.4